[PROC. OF JSCE No. 408/V-11 (Concrete Eng. and Pavements) August 1989]

AE OBSERVATION IN THE PULL-OUT PROCESS OF SHALLOW HOOK ANCHORS

By Masayasu OHTSU, Mitsuhiro SHIGEISHI** and Hiroyuki IWASE****

A source inversion procedure for determining crack types and crack orientations is proposed as the quantitative waveform analysis of acoustic emission (AE), based on the integral representation and the moment tensor. The procedure is applied to AE events monitored during the pull-out tests of hooked anchor-bolts from concrete block.

The integral representation is first applied to the stress analysis by the boundary element method (BEM). It confirms that the failure surface is generated as perpendicular to the direction of the maximum tensile stress.

AE waveforms detected at five sensor locations during the failure process are analyzed by the source inversion procedure. Crack kinematics determined are in good agreement with experimental findings.

Keywords : *acoustic emission, pull-out test, source inversion, crack kinematics, boundary element method*

1. INTRODUCTION

Embedded anchors have widespread applications in the engineering design due to increased demand for inserts and fixings in concrete structures. The bearing capacity and failure behaviour of anchors are often checked by pull-out testing. The pull-out test is also presently utilized as a means for testing the strength of concrete in nondestructive evaluation[1]. In these respects, major efforts are associated with clarifying the failure process in the pull-out test.

For the calculation of the bearing capacity of anchors, analytical investigations on the failure process were intensively carried out in the early 1980's. Pull-out behaviors of anchors were studied by using the continuous finite element method (FEM)[2,3]. Based on the theory of plasticity, the modified Mohr-Coulomb criterion was employed along with a sophisticated triaxial stress criterion, which includes concrete crushing. In these FEM studies, the failure of anchors was reported to be induced by crushing of concrete, which developed the spatially distributed failure of concrete. This failure mode is, however, not found in experiments, but a single failure surface is observed. To overcome this discrepancy, the concept of fracture mechanics has been introduced. The propagation of a crack from the edge of anchor is studied by a discrete crack approach of FEM[4] and an integral equation approach[5].

The anchorage in concrete is classified into three groups, depending on the way how the load is transferred into concrete[4]. In hook anchors, the load is considered to be transferred by compressive stress in concrete, while the load is transferred by adhesion in adhesive anchors and by friction in

* Member of JSCE, Dr. Eng., Associate Professor, Department of Civil and Environmental Engineering, Kumamoto University (2-39-1 Kurokami, Kumamoto 860)

** Member of JSCE, Graduate Student, Department of Civil and Environmental Engineering, Kumamoto University, On leave from Kawada Construction Co. Ltd.

*** Member of JSCE, Adjunct Lecturer, Department of Civil Engineering, Gifu University (1-1 Yanagido, Gifu 501-11)

expansion anchors. In the present study, acoustic emission (AE) observation is performed in the pull-out process of shallow hook anchors.

Source characterization of AE has been investigated to obtain quantitative information on fracture mechanisms of cracks[6] and the theoretical treatment is summarized as a generalized theory of AE[7]. The theory is based on the integral representation, which is also applied to stress analysis by the boundary element method (BEM) in this paper. To investigate crack kinematics of general AE sources, the moment tensor analysis is introduced[8]. On the basis of these theories, a source inversion procedure is applied to AE waveforms detected in the pull-out tests of the shallow hook anchor. Note that results of the source location analysis in the same series of experiments were already reported elsewhere[9]. In this research, pull-out experiments were performed in Gifu University and the analysis of AE data was carried out in Kumamoto University.

2. THEORETICAL BACKGROUND

(1) Integral representation and BEM formulation

A mathematical description of displacement solution $u_i(\boldsymbol{x}, t)$ in elastodynamics is obtained by the following integral representation[6],

$$u_i(\boldsymbol{x}, t)=\int_S [G_{ij}(\boldsymbol{x}, \boldsymbol{y}, t)*t_j(\boldsymbol{y}, t)-T_{ij}(\boldsymbol{x}, \boldsymbol{y}, t)*u_j(\boldsymbol{y}, t)]dS, \quad (1)$$

where S denotes the boundary surface surrounding a body and $*$ means a convolution integral in respect to time. $t_j(\boldsymbol{y}, t)$ and $u_j(\boldsymbol{y}, t)$ are the traction and the displacement on boundary S, respectively. $G_{ij}(\boldsymbol{x}, \boldsymbol{y}, t)$ is Green's function, which implies the displacement in the x_i direction at point $\boldsymbol{x}$ and at time t due to an impulse force in the x_j direction at point $\boldsymbol{y}$ and at time $t=0$. T_{ij} is the traction associated with Green's function and is represented in the case of isotropic elastic materials, as follows;

$$T_{ij}=E\nu\, G_{ik,k}n_j/[(1+\nu)(1-2\nu)]+E[G_{ij,k}n_k+G_{ik,j}n_k]/(2+2\nu), \quad (2)$$

where, E is Young's modulus and ν is Poisson's ratio. n_j is an outward unit normal to the boundary surface. The comma means the spatial derivative of Green's function, as $\partial G_{ij}/\partial y_k$.

Eq. (1) is the basic representation in the boundary element method (BEM). In elastostatic problems, the convolution integral is converted into just a multiplication. Thus, it becomes,

$$u_i(\boldsymbol{x})=\int_S [G_{ij}(\boldsymbol{x}, \boldsymbol{y})t_j(\boldsymbol{y})-T_{ij}(\boldsymbol{x}, \boldsymbol{y})u_j(\boldsymbol{y})]dS. \qquad (\boldsymbol{x} \text{ in } D,\ \boldsymbol{y} \text{ on } S) \quad (3)$$

Eq. (3) implies that displacement $u_i(\boldsymbol{x})$ at any points located inside the body can be calculated by the surface integration on S, if all tractions and displacements on boundary S are prescribed. Stress components σ_{ij} are obtained, by substituting eq. (3) into the following equation,

$$\sigma_{ij}=E\nu\, u_{k,k}\delta_{ij}/[(1+\nu)(1-2\nu)]+E[u_{i,j}+u_{j,i}]/(2+2\nu). \quad (4)$$

The integral equation of the BEM is obtained, by the limiting process where interior point $\boldsymbol{x}$ approaches to the boundary point. Thus, we have a singular integral equation,

$$cu_i(\boldsymbol{x})=\int_S [G_{ij}(\boldsymbol{x}, \boldsymbol{y})t_j(\boldsymbol{y})-T_{ij}(\boldsymbol{x}, \boldsymbol{y})u_j(\boldsymbol{y})]dS. \qquad (\boldsymbol{x} \text{ and } \boldsymbol{y} \text{ on } S) \quad (5)$$

where c is the configuration coefficient obtained from the limiting process. On the smooth boundary, c is identical to 1/2. These coefficients are easily determined from eliminating rigid motion in eq. (5). Note that point $\boldsymbol{x}$ in eq. (5) is located on the boundary S, while point $\boldsymbol{x}$ in eqs. (1) and (3) is located inside the body. Thus, eq. (5) constitutes a boundary integral equation in respect with unknown quantities of either traction $t_j(\boldsymbol{y})$ or $u_j(\boldsymbol{y})$. Stresses inside the body are computed from eqs. (3) and (4), after all tractions and displacements are determined from solutions of eq. (5).

(2) Moment tensor and source inversion

AE waveform $u_i(\boldsymbol{x}, t)$ due to displacement discontinuity $b_k(\boldsymbol{y}, t)$ on crack surface F can be obtained from eq. (1), assuming two boundary surfaces F^+ and F^-. Taking into account the continuity of stress and the displacement discontinuity on surfaces, AE waveform $u_i(\boldsymbol{x}, t)$ is represented[7],

$$u_i(\boldsymbol{x}, t)=\int_F T_{ik}(\boldsymbol{x}, \boldsymbol{y}, t)* b_k(\boldsymbol{y}, t)dS. \quad (6)$$

Here $b_k=u_k^+-u_k^-$ and the outward normal on the boundary F is defined on surface F^-. Note that the surface integral is converted into that on F, because of the homogeneous boundary condition on S. For a small crack, the space and time dependencies of displacement discontinuity $b_k(\boldsymbol{y}, t)$ are separated, as follow ;

$$u_i(\boldsymbol{x}, t)=T_{ik}(\boldsymbol{x}, \boldsymbol{y}, t)*\int_F b_k(\boldsymbol{y}, t)dS=T_{ik}(\boldsymbol{x}, \boldsymbol{y}, t)bl_k*S(t), \quad (7)$$

where $\int_F b_k(\boldsymbol{y}, t)dS=bl_kS(t)$.

Substituting eq. (2) into eq. (7), the moment tensor representation is obtained[8],

$$u_i(\boldsymbol{x}, t)=G_{ip,q}(\boldsymbol{x}, \boldsymbol{y}, t)m_{pq}*S(t), \quad (8)$$

where

$$m_{pq}=b[E\nu l_k n_k \delta_{pq}/(1+\nu)/(1-2\nu)+E(l_p n_q+l_q n_p)/(2+2\nu)]. \quad (9)$$

In eqs. (7) and (9), b represents the crack volume, vector l_k denotes the direction of crack movement, and $S(t)$ denotes the time dependency of crack formation which is normally called a source-time function. If appropriate function $S(t)$ and crack volume b are prescribed, a simulation analysis of AE waveforms can be performed by eq. (8). An application of the simulation analysis was already reported in the debonding process of stainless steel overlay[10),11)].

Taking into account only the dominant term of P wave in eq. (8), an approximated representation of the first motion is obtained[12],

$$u_i(\boldsymbol{x})=r_i r_p r_q m_{pq}/(4\pi\rho R v_p^3). \quad (10)$$

Here R is the distance from source point $\boldsymbol{y}$ to observation point $\boldsymbol{x}$ and r_i is its direction cosine. Because only the amplitude of the first motion (P wave) is taken into account, the time dependency is omitted.

When elastic waves due to one AE event are detected at several locations, the amplitudes of the first motions correspond to the left-hand-side of eq. (10), after the reflection calibration. Since the source location procedure can provide information on distance R and direction cosine r_i, eventually a set of linear algebraic equations is obtained with unknown values of m_{pq}. The moment tensor is a symmetric second rank tensor. Six independent components are to be determined from eq. (10). In the proposed procedure, however, only relative values of tensor components are necessary and ratios of eigenvalues are essential. It implies that the minimum number of observation points becomes five.

Because moment tensor m_{pq} is the second rank tensor, the determination of the principal components is readily performed by the eigenvalue analysis. Characteristics of eigenvalues for a pure tensile crack and a pure shear crack are clarified[12),13)]. For eigenvalues of a tensile crack, components can be decomposed into deviatoric components and hydrostatic mean components. In seismology, deviatoric components are known as the compensated linear vector dipole (CLVD)[14]. In practical situations, AE sources may consist of a tensile crack and a shear crack. The eigenvalue analysis of the moment tensor leads to a technique to decompose eigenvalues into three components[15]. Setting the ratio of shear component as $(X, 0, -X)$, that of CLVD component as $(Y, -0.5\ Y, -0.5\ Y)$, and mean component as Z, the ratios of eigenvalues are uniquely decomposed,

$$1.0=X+Y+Z,$$

$$\text{The intermediate eigenvalue/the maximum eigenvalue} = 0-0.5\ Y+Z, \quad (11)$$

$$\text{The minimum eigenvalue/the maximum eigenvalue} = -X-0.5\ Y+Z.$$

The decomposition in eq. (11) is so practical that it includes no elastic constants. On the basis of the present decomposition, a simple criterion is proposed for the classification of crack types. For example, when ratio X is bigger than 50 %, AE source is referred to as a shear crack. In the reverse case, AE source must be of a tensile crack.

After determining the crack type, the direction of crack motion is derived from eigenvectors[12]. Since the eigenvector for the maximum eigenvalue directs the direction of tensile motion, crack orientation of tensile type is easily determined. For a shear crack, either the direction of crack motion l_k or unit normal n_k is determined from the sum of the first and the third eigenvectors. Vector l_k is vertical to n_k for a shear crack. Consequently, if the one direction is determined, the other is easily identified.

All treatments discussed above are associated with only the theory of elasticity, while concrete materials are known as inhomogeneous and inelastic. The reason, why the treatments are available for the analysis of AE, results from the wavelength of AE waves in concrete. Theoretically, the scattering of elastic waves due to obstacles is observed in only the case that the wavelength of propagating wave is shorter than the physical size of the obstacle. Taking into account the wave velocity in concrete (a typical value is 4 000 m/s) and the frequency components of AE (a typical frequency is 50 kHz ; the corresponding period is 0.02 msec), a wavelength corresponds to 80 mm. This result shows that the effect of the inhomogeneity in concrete is not dominant in the cases that the sizes of aggregates are smaller than 80 mm. It implies that AE waveforms detected are less sensitive to the inhomogeneity in normal concrete.

3. EXPERIMENTS AND ANALYSIS

(1) Experiments

AE source inversion procedure was applied to AE waveforms detected in the pull-out test of hooked anchor-bolt from concrete block. AE observation was carried out in two concrete blocks of dimension 0.6 m×0.6 m×0.3 m, which are referred to as specimen A and specimen B. Mix proportion of concrete is shown in Table 1. The size of maximum gravel was 15 mm and the water-reducing agent was added at 2 % of cement weight. Mechanical properties are indicated in Table 2. Strengths were determined by using three standard cylinder samples of 10 cm diameter and 20 cm height at 28 days. Results are indicated along with mixing conditions of air content and slump value. The velocity of P wave is determined from the travelling duration.

A configuration of an anchor-bolt is shown in Fig. 1. A washer of 44 mm diameter and 3.2 mm thickness corresponds to an anchor plate. Pull-out load is transferred by a post-tensioning steel bar of 17 mm diameter, which is fixed to a nut of 27 mm thickness. This system was embedded in the concrete block at 5 cm depth. To remove the bond resistance between a post-tensioning bar and surrounding concrete, the steel bar was wrapped up with polyethylene sheet.

An experimental set-up is shown in Fig. 2. The post-tensioning steel bar was pulled out by employing a center-hole jack. Pull-out load and displacements on the top surface were measured by a load cell and displacement meters, respectively. During the failure process of the pull-out test, AE events were detected and recorded. Observing AE activity, pull-out force was loaded or unloaded to prevent from reaching sudden final failure.

Five AE sensors were attached to the concrete block to detect AE waveforms during the pull-out process. Sensors were of resonant type with 150 kHz resonance. Sensor locations are shown in Fig. 3. Total amplification of AE signals was 60 dB and the frequency range recorded was 30 kHz to 80 kHz. AE waveforms detected at sensor locations were recorded by a digital memory, which converted analog records to digital records at 1 MHz sampling frequency.

(2) Analytical model

Although analytical and numerical solutions in the pull-out tests were reported[2)~5)], these are related

Table 1 Mix proportion of concrete.

W/C (%)	s/a (%)	unit weight (kg/m^3) W	C	S	G
52	50	182	350	866	866

Table 2 Mixing and mechanical properties of concrete.

air (%)	slump (cm)	compressive strength(Mpa)	tensile strength(Mpa)	P wave velocity(m/s)
4	14	45.5	3.2	4040

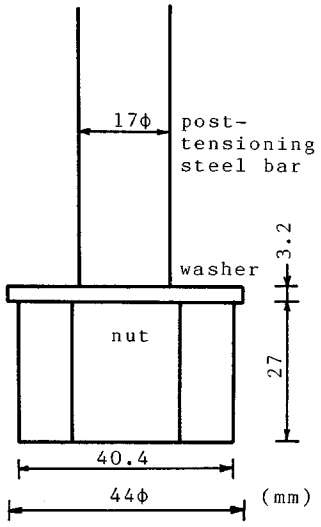

Fig. 1 Configuration of anchor-bolt.

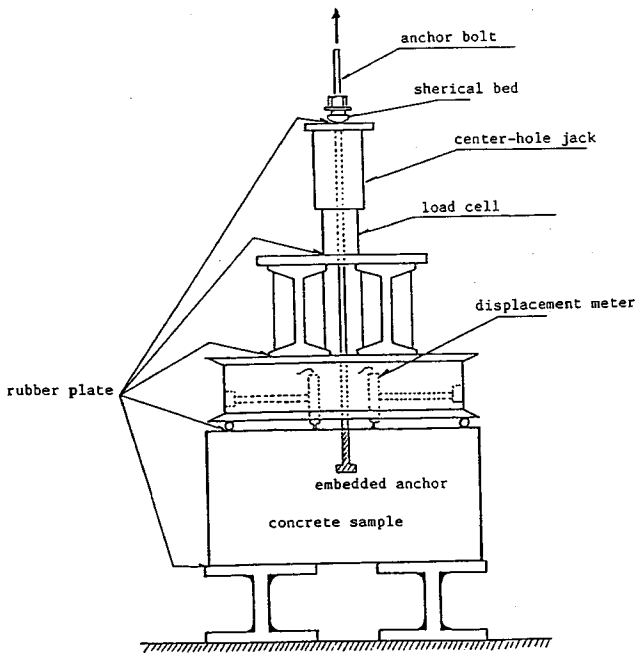

Fig. 2 Experimental set-up for the pull-out test.

with the pull-out (LOK) test and the apex angle between the anchorage and the reacting support is quite small. As can be seen in Fig. 2, the apex angle in the experiment is more than 60°, and thus no analytical solution is available. Therefore, numerical analysis was attempted. An analytical model of the BEM is shown in Fig. 4. The one-third upper portion of the symmetrical half block was considered as the model, of which boundary was devided into 52 elements. Since the constant element was employed in the BEM analysis, the representative point of each element is denoted in the center of the element with solid circle. Note the bottom boundary of the model is not closed. Since Green's function G_{ij} in an infinite

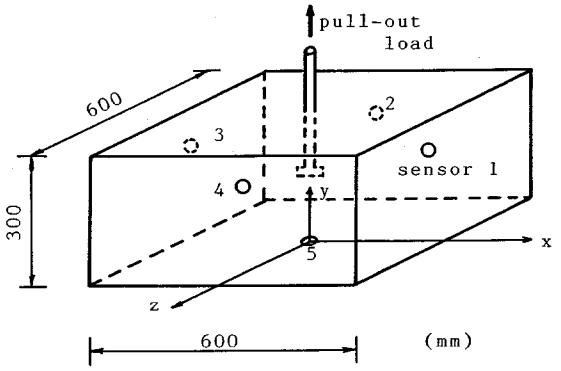

sensor 1:(300, 230, 50) 2:(-50, 200,-300)
sensor 3:(-300, 200, -50) 4:(50, 230, 300)
sensor 5:(0, 0, 0)

Fig. 3 AE sensor locations in the concrete block.

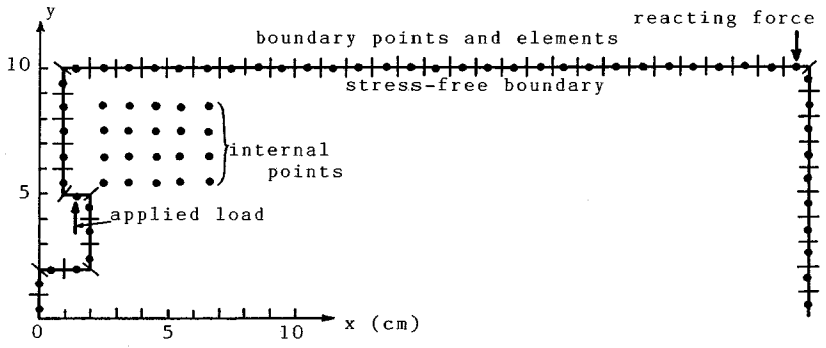

Fig. 4 BEM model analyzed.

space is normally employed in the BEM analysis, the bottom portion of this model is assumed as connected with the infinite space and no boundary conditions are specified on it. The boundary conditions on the elements are prescribed at boundary points, where stresses are free except for two loading points in the figure. Locations of an applied load due to the pull-out of an anchor-bolt and the reacting force at the support are indicated by an arrow.

The integration of each element was carried out by the Gaussian 4-point scheme. From experimental data, Young's modulus of 32.3 GPa and Poisson's ratio of 0.2 were utilized. To compute stress distribution from eqs. (3) and (4), 20 internal points were selected. These are shown by solid circles.

4. RESULTS AND DISCUSSION

The ultimate loads in specimen A and specimen B were 4.1 ton and 4.2 ton, respectively. According to large-scale pull-out tests, three phases of the failure process and the shape of failure surfaces were known[16]. In the phase 1, the initiation of circumferential cracking near the upper edge of the anchor plate is observed at a approximately 1/3 of the ultimate load. The phase 2 corresponds to the completion of circumferential cracking from the anchor edge to the reaction support at approximately 2/3 of the ultimate load. Beginning at about 80 % of the ultimate load, the phase 3 promotes shear failure of matrix and the degradation of aggregate interlock. The shape of failure surface is closely related to the apex angle between the anchor edge and the reaction support. For the low apex angle, the failure surface follows the shape of a conical frustum. At the high apex angle, a trumpet-shaped frustum is observed. In the present experiments, the apex angle is bigger than 60°, but the depth of anchor-bolt is rather shallow. Results of the observed failure surfaces were of thin trumpet-shaped frustum centered by the anchor plate in both specimens.

Although the integral equation similar to the BEM was solved by using the linear-elastic fracture analysis[5], the elastic stress analysis was only performed by the BEM to quantify the mechanism at the phase 1. Since the ultimate load of 4.2 ton corresponds to 27.0 MPa (276 kgf/cm^2) traction at the bottom of the anchor plate, traction of 9.8 MPa (100 kgf/cm^2) was applied at loading points in the model of Fig. 4. Results of the stress analysis is shown in Fig. 5. Principal stresses are indicated in the principal direction. In the same figure, side views of failure surfaces observed in both Specimen A and Specimen B are

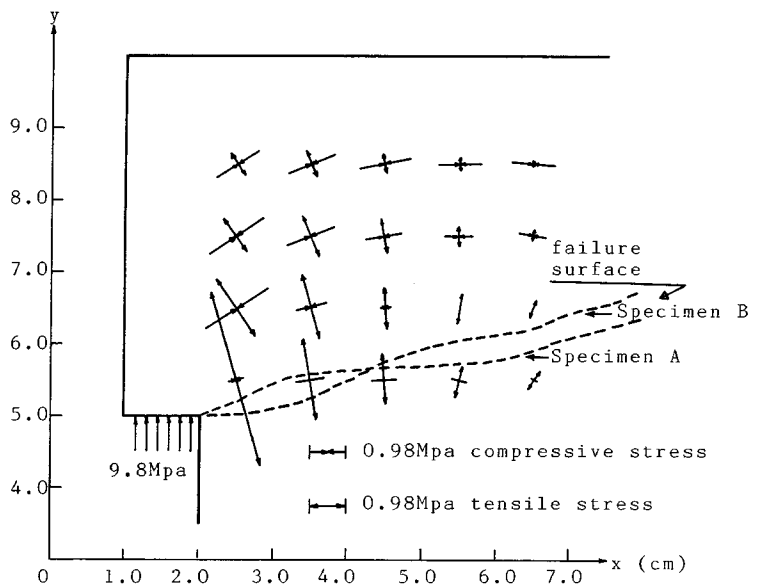

Fig. 5 Stress distribution near the anchor plate at the pull-out stress of 9.8 MPa.

indicated by broken curves. At the closest point to the anchor edge, the highest tensile stress of about 4.9 MPa (50 kg/cm^2) is observed. Since the tensile strength of concrete was 3.2 MPa, it can be predicted that the tensile failure is to be generated in advance to this load level. Note that the direction of tensile stress is in remarkable agreement with the crack opening direction of the observed failure surfaces. Other directions of tensile stress on the bottom line are also coincident with the opening direction of the failure surface. It confirms the failure mechanisms suggested by Stone[16]. There is a debate whether the dominant failure mechanism in the pull-out test is tensile or compression, because the nondestructive evaluation of compressive strength is performed by the pull-out test[1]. The result of the analysis suggests that the failure process is governed by tensile motion.

An example of AE waveforms detected is shown in Fig. 6. All AE waveforms were transferred from a digital memory to a microcomputer via GP-IB interface and stored onto a disk. After the experiments were completed, waveform data were displayed on a CRT screen. P wave arrival time and the amplitude of the first motion were read. In some waveform data, the arrival time and the amplitude of first motion were very ambiguous because of high background noise. Since the accuracy of the source location and the applicability of the moment tensor analysis are directly related with the clear discrimination of the first motions in AE signals, the analysis of these data was resigned. By using the source location algorithm[17),18)], locations of AE sources were determined. According to the previous study, the accuracy of the location is known within 1 cm. Moment tensor components were obtained from eq. (10). Although the accuracy of the source inversion was already known as less than 10 % error in the numerical analysis[15)], the effects of experimental conditions on the moment tensor analysis is not clarified yet. Further studies on these effects, such as noise level, material inhomogeneity, microstructure of concrete, and AE monitoring devices are surely needed, before attempting in situ applications.

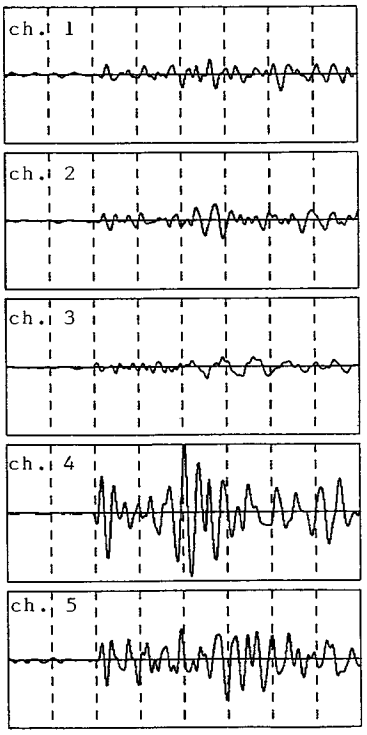

Fig. 6 An example of AE waveforms detected in the experiment.

Since five-channel system was utilized, relative values in respect to the maximum value were determined. Then, the eigenvalue analysis was performed. By employing eq. (11), shear ratio X of all detected AE events were computed. Originally, we considered that the event of which X ratio is more than 50 % should belong to shear types. However, X ratios of some events were larger than 45 % but less than 55 %. Since analytical errors of results are inevitable, these events may not be correctly classified. Therefore, these events were separately taken into consideration. The events of which X ratio was more than 55 % were classified into shear type, while those of X less than 45 % were classified into tensile. Results of the source location and the crack-type classification are shown in Fig. 7. The graphs show the load-history curve. AE events are indicated at the time when each AE event is detected in respect to the horizontal axis. These events are classified into tensile type (indicated by a cross symbol), shear type (a square symbol), and combined type (a cross symbol with solid circle). To see the spatial and time sequences of AE sources, AE events are plotted against the radial distance from the anchor-bolt.

Fig. 7 (a) shows results in the case of specimen A. AE events located are seen just prior to the ultimate load. Although a few AE events of tensile type are observed from pre-ultimate range to the early stage of softening, dominant mechanisms are of shear motion near the anchorage. It may imply the bond slip between the anchor plate and concrete. It is clearly observed that AE events of tensile type propagate in

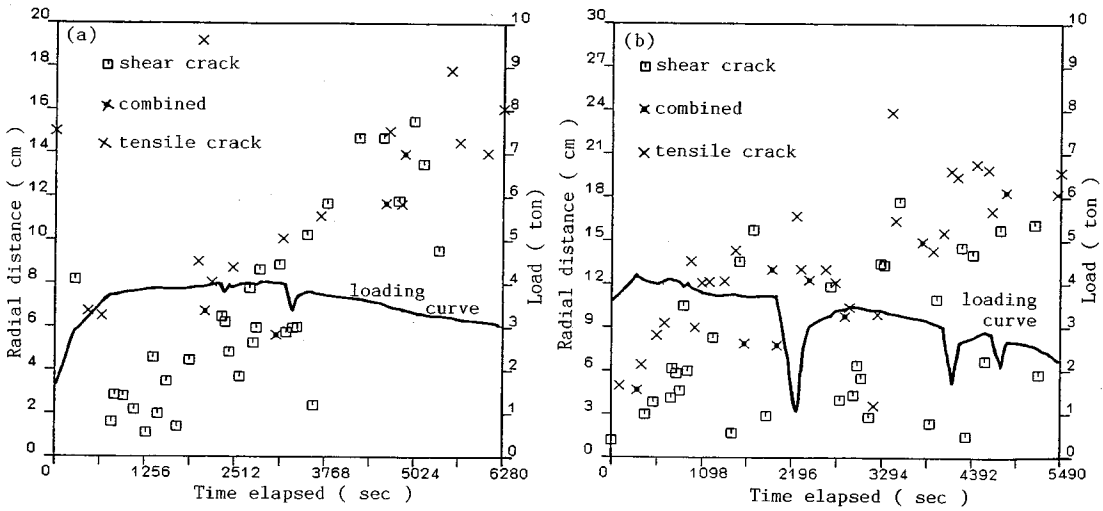

Fig. 7 Load history and the spatial-time sequences of AE events in (a) specimen A and in (b) specimen B.

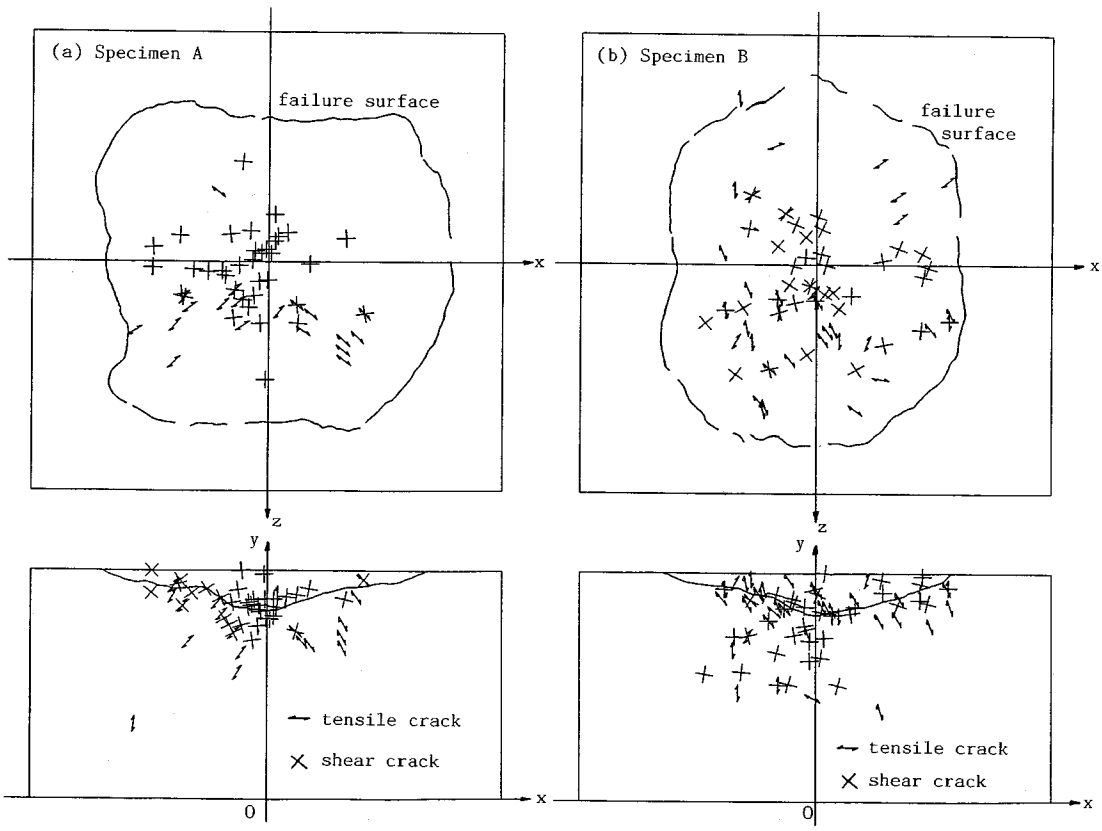

Fig. 8 Top and side views of AE source locations with crack type and crack orientation in (a) specimen A and in (b) specimen B.

the radial direction during the failure process. Fig. 7(b) shows the results of specimen B. AE events of tensile type propagate in the radial direction, while AE events of shear type are restrictively generated near the anchorage during the whole process.

Because all AE events during the pull-out process can not be recorded, the precise investigation of the

failure process is not the easy task. In specimen A, 59 events were located and analyzed out of only 117 events. 77 out of 119 events were analyzed in specimen B. Therefore, the experimental confirmation of the phase 1 process is not clear. Still, a few AE events of tensile type are certainly observed prior to the ultimate load in both specimens.

The top and side views of these AE sources are shown in Fig. 8. The final failure surfaces are shown by solid curves. AE sources are plotted at their locations with the crack type and the direction of crack motion. Since either vector n_k or vector l_k was determined from the eigenvectors for a shear crack, two possible vertical directions are indicated. For a tensile crack, the direction of opening is denoted. For the events of which X ratios vary between 45 % and 55 %, both directions of tensile motion and shear motion are plotted. From these graphes, it is observed that the opening directions of tensile type are not only vertical to the final failure surface in the side views, but also of radially distributed from the anchor-bolt in the top views. It shows that the directions of tensile motion determined by the AE source inversion are in good agreement with those of the crack opening observed. AE events of shear type are intensely distributed around the bottom of anchor-bolt and the direction of shear motion are nearly parallel to the failure surface in the side views.

5. CONCLUSION

(1) The source inversion procedure proposed is applied to AE events monitored during the pull-out tests of shallow hook anchor-bolt from concrete block. Thus, the failure process of the pull-out process is studied by the BEM analysis and the source inversion of AE.

(2) Results of the BEM analysis confirms that the tensile failure occurs at approximately one-third of the ultimate load. The direction of the maximum tensile stress is of high apex angle and is in good agreement with the failure surfaces observed.

(3) Crack kinematics determined are in good agreement with experimental findings. Crack orientations of AE events due to tensile motion are approximately vertical to the final failure surface. Cracks of tensile type propagate radially from the anchorage to the reaction support, while those due to shear type are restrictively observed near the anchorage. It implies that the slip motions occur at the bottom of the anchor plate.

ACKNOWLEDGEMENT

The authors wish to thank Profs. W. Koyanagi and K. Rokugo in the Department of Civil Engineering, Gifu University, for their support to complete this research. Their critical comments and fruitful discussion were extremely valuable.

REFERENCES

1) Akashi, T. and Amasaki, S. : State-of-the-Art Report on Nondestructive Testing of Concrete, Concrete Journal, Vol. 23, No. 12, JCI, pp. 11-20, 1985 (in Japanese).
2) Ottosen, N. S. : Nonlinear Finite Element Analysis of Pull-Out Test, Journal of Structural Division, Vol. 107, No. ST 4, Proc. of ASCE, pp. 591-603, 1981.
3) Peier, W. H. : Model for Pull-Out Strength of Anchors in Concrete, Journal of Structural Engineering, Vol. 109, No. 5, Proc. of ASCE, pp. 1155-1173, 1983.
4) Eligehausen, R. and Sawabe, G. : Anchorage of Inserts and Bolts, 3 rd Draft of RILEM Technical Committee 90, Fracture Mechanics of Concrete-Application, Chapter 13.
5) Miller, G. R. and Keer, L. M. : Approximate Analytical Model of Anchor Pull-Out Test, J. Applied Mechanics, Trans. ASME, Vol. 49, No. 4, pp. 768-772, 1983.
6) Ohtsu, M. : Source Mechanism and Waveform Analysis of Acoustic Emission in Concrete, J. Acoustic Emission, Vol. 1, No. 2, pp. 103-112, 1982.
7) Ohtsu, M. and Ono, K. : A Generalized Theory of Acoustic Emission and Green's Functions in A Half Space, J. Acoustic Emission, Vol. 3, No. 1, pp. 27-40, 1984.

8) Ohtsu, M. : Mathematical Theory of Acoustic Emission and Moment Tensor Solution, J. Soc. Mat. Sci. Japan (Zairyou), Vol. 36, No. 408, pp. 1025-1031, 1987 (in Japanese).
9) Iwase, H., Tsumagari, T., Rokugo, K. and Koyanagi, W. : Pull-Out Tests of Anchor-Bolt and Detection of Acoustic Emission, Proc. JCI, Vol. 9, No. 2, pp. 573-578, 1987 (in Japanese).
10) Ohtsu, M., Yuyama, S. and Imanaka, T. : Theoretical Treatment of Acoustic Emission Sources in Microfracturing due to Disbonding, J. Acoust. Soc. Am., Vol. 82, No. 2, pp. 506-512, 1987.
11) Yuyama, S., Imanaka, T. and Ohtsu, M. : Quantitative Evaluation of Microfracture due to Disbonding by Waveform Analysis of Acoustic Emission, J. Acoust. Soc. Am., Vol. 83, No. 3, pp. 976-983, 1988.
12) Ohtsu, M. : Determination of Crack Orientation by Acoustic Emission, Materials Evaluation, Vol. 45, No. 9, pp. 1070-1075, 1987.
13) Aki, K. and Richards, P. G. : Quantitative Seismology Theory and Methods, W. H. Freeman and Company, San Francisco, 1980.
14) Knopoff, L. and Randall, M. J. : The Compensated Linear-Vector Dipole : A Possible Mechanism for Deep Earthquakes, J. Geophys. Res., Vol. 75, No. 26, pp. 4957-4963, 1970.
15) Ohtsu, M. : Source Inversion of Acoustic Emission Waveform, Proc. of JSCE, No. 398/I-10, pp. 71-79, 1988.
16) Stone, W. C. and Carino, N. J. : Deformation and Failure in Large-Scale Pullout Tests, ACI Journal, Vol. 80, No. 6, pp. 501-513, 1983.
17) Niwa, Y., Kobayashi, S. and Ohtsu, M. : Studies of Source Location by Acoustic Emission, Proc. JSCE, No. 276, pp. 135-147, 1978 (in Japanese).
18) Ohtsu, M. and Ono, K. : AE Source Location and Orientation Determination of Tensile Cracks from Surface Observation, NDT International, Vol. 21, No. 3, pp. 143-150, 1988.

(Received August 13 1988)